CODEN [USA]: IAJPBB ISSN: 2349-7750

INDO AMERICAN JOURNAL OF
PHARMACEUTICAL SCIENCES

http://doi.org/10.5281/zenodo.1193652

Available online at: http://www.iajps.com Research Article

ELECTROCHEMICAL BIOSENSOR STUDIES OF NITROKETENE DITHIOACETAL -METAL COMPLEXES

J. Kavitha[1], S. Aarthi[1], S. Bhuvaneshwari[1], L. Sakthikumar[2], R. Mahalakshmy[3]

[1]Department of Chemistry, V.V.Vanniaperumal College for Women, Virudhunagar, Tamilnadu, India

[2]Department of Chemistry, Saiva Bhanu Kshatriya College, Aruppukottai, Tamilnadu, India

[3]Post Graduate and Research Department of Chemistry, Thiagarajar College, Madurai, Tamilnadu, India

Abstract:

Biosensors can be also divided into several categories based on the transduction process, such as electrochemical, optical, piezoelectric, and thermal/calorimetric biosensors. Among these various kinds of biosensors, electrochemical biosensors are a class of the most widespread, numerous and successfully commercialized devices of biomolecular electronics. Carbon and carbon based materials such as carbon nanotubes (single and multi-walled), graphene oxides, and fullerenes are good materials for various fields like battery applications, and biosensors due to their higher electrical conductivity, high mechanical strength, high surface area, thermal stability etc. On the other hand, conducting polymers have attracted behavior owing to their electrocatalytic activity and higher conductivity compared to those of carbon based materials. Among those conducting polymers, polyindole (PIn) is a great one with more advantages, such as its mechanical flexibility, light weight and low cost. Metal composites such as Mn_2O_3, Fe_3O_4, Ti_2O_3, Co_3O_4, NiO, and Cr_2O_3 have attracted fantastic attention in current years owing to their potential in environmental monitoring, sensor, drug delivery, photocatalysis, biomedical diagnosis, and energy storage applications These interesting properties revealed one of the greatest hopeful aspirants for their industrial applications. Among these metal oxides, Ti_2O_3 metal oxide have been commonly used in the invention of electrochemical biosensors, semiconductors, and in making electrical goods due to its large strong catalytic ability, adsorptive ability and surface area. Also it is cheaper than the traditional catalysts and these nanoparticles is easily incapacitating on the external of the metal electrodes, but secure them directly on the carbon electrode surface is quite difficult. The new metal ligand complex of NKDA-Metal[(7)] was the as-synthesized NM has high dispersible property in water. The modified SPCE of NKDA – Zinc complex have electro-catalytic activity towards the detection of L-Met. The electrochemical behaviors of the NZ/SPCE were examined using cyclic voltammetry, and differential pulse voltammetry (DPV). The antibacterial activity of the complex was evaluated using Disc-Diffusion method.

Key words: *Metal-drug complexes, Electrochemical study, Biosensor, Nitroketene dithioacetal complex, antibacterial activity.*

Corresponding author:

J. Kavitha,

Assistant Professor,
Department of Chemistry,
V.V.Vanniaperumal College for Women,
Virudhunagar-626 001.Tamilnadu,India.
Email Id: kavithasakthikumaar@gmail.com
Mobile: 9047108750

QR code

Please cite this article in press as J. Kavitha et al., ***Electrochemical Biosensor Studies of Nitroketene Dithioacetal -Metal Complexes****, Indo Am. J. P. Sci, 2018; 05(02).*

1.1.INTRODUCTION:

In the era of nanotechnology, metal nanoparticles (NPs) have played an important role in the development of new biosensors and/or in the enhancement of existing biosensing techniques to fulfill the demand for more specific and highly sensitive biomolecular diagnostics. The unique physicochemical properties of such metals at the nanoscale have led to the development of a wide variety of biosensors, such as: (i) nanobiosensors for point of care disease diagnosis, (ii) nanoprobes for *in vivo* sensing/imaging, cell tracking and monitoring disease pathogenesis or therapy monitoring and (iii) other nanotechnology -based tools that benefit scientific research on basic biology [1-8]. In fact, NPs are, in general, one of the most common nanotechnology-based approaches for developing biosensors, due to their simplicity, physiochemical malleability and high surface areas [9]. They can measure between 1 to 100 nm in diameter, have different shapes and can be composed of one or more inorganic compounds, such as noble metals, heavy metals, iron, *etc*. The majority of them exhibit size-related properties that differ significantly from those observed in microparticles or bulk materials. Depending on their size and composition we can observe peculiar properties, such as quantum confinement in semiconductor nanocrystals, surface plasmon resonance in some metal NPs and super paramagnetism in magnetic materials. Metal NPs, in particular gold and silver NPs, are among the most extensively studied nanomaterials and have led to the development of innumerous techniques and methods for molecular diagnostics, imaging, drug delivery and therapeutics. Most of their unique physicochemical properties at the nanoscale, such as Localized Surface Plasmon Resonance (LSPR), have been explored for the development of new biosensors. Some recent reports have addressed specific bio-application for noble metal NPs, such as molecular diagnostics and therapy [10,11] or cancer applications [12], and others have focused on the bio-applications of a specific type of metal NP.

1.2. The application of nanomaterials in electrochemical sensors

Nanotechnology has recently become one of the most exciting forefront fields in analytical chemistry. A wide variety of nanoscale materials of different sizes, shapes and compositions at the 1-100 nm scale, are now available. Metal and polymeric nanoparticles were applied in this work for designing novel sensing systems, enhancing the performance of bioanalytical assays and improving the visualisation of biointeractions occurring on sensing surfaces. A novel nanoparticulate formulation of the conducting polymer polyaniline (PANI) was applied for the development of a chemical sensor device capable of detecting both ascorbic acid and hydrogen peroxide. The "nanoPANP-modified electrode showed enhanced electrocatalysis over traditional bulk PANI films for hydrogen peroxide. Inkjet printing deposition of this highly processable nanomaterial onto screen-printed electrodes was also demonstrated for simple and rapid sensor device production. A biosensor can be defined as a device incorporating a biological sensing element connected to a transducer to convert an observed response into a measurable signal, whose magnitude is proportional to the concentration of a specific chemical or set of chemicals [13]. According to the receptor type, biosensors can be classified as enzymatic biosensors, genosensors, immunosensors, etc. Biosensors can be also divided into several categories based on the transduction process, such as electrochemical, optical, piezoelectric, and thermal/calorimetric biosensors. Among these various kinds of biosensors, electrochemical biosensors are a class of the most widespread, numerous and successfully commercialized devices of biomolecular electronics [14]. Carbon and carbon based materials such as carbon nanotubes (single and multi-walled), graphene oxides, and fullerenes are good materials for various fields like battery applications, and biosensors due to their higher electrical conductivity, high mechanical strength, high surface area, thermal stability etc., [15]. On the other hand, conducting polymers have attracted behavior owing to their electrocatalytic activity and higher conductivity compared to those of carbon based materials [16]. Among those conducting polymers, polyindole (PIn) is a great one with more advantages, such as its mechanical flexibility, light weight and low cost [17]. Metal composites such as Mn_2O_3, Fe_3O_4, Ti_2O_3, Co_3O_4, NiO, and Cr_2O_3 have attracted fantastic attention in current years owing to their potential in environmental monitoring, sensor, drug delivery, photocatalysis, biomedical diagnosis, and energy storage applications [18-20]. These interesting properties revealed one of the greatest hopeful aspirants for their industrial applications. Among these metal oxides, Ti_2O_3 metal oxide have been commonly used in the invention of electrochemical biosensors [21], semiconductors, and in making electrical goods due to its large strong catalytic ability, adsorptive ability and surface area.[22] Also it is cheaper than the traditional catalysts and these nanoparticles is easily incapacitating on the external of the metal electrodes, but secure them directly on the carbon electrode surface is quite difficult.[23]

2.0. EXPERIMENTAL SECTION

2.1. Synthesis of Dipotassium salt of 2-nitro-1,1-ethylene dithiolate (3)

To a well stirred and ice cooled solution of carbon disulphide **(2)** (23mL, 0.41mole) and nitromethane **(1)** (18mL,0.33mole) solution of potassium hydroxide (39g) in 95mL of HPLC grade methanol was added drop by drop for 40 minutes using a pressure equalizing funnel. The stirring was continued for 3hrs at 0^0c to - 5^0c. The reddish brown colour powder formed in the reaction mixture was quickly filtered and washed with dry methanol (3x10mL) followed by dry ether (3x10mL) to yield 38.0g (55.2%) of reddish brown colour powder[6] **(3)**. The salt **(3)** was quickly transferred into brown colour sample bottle to avoid photodecomposition.

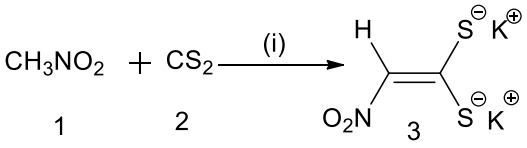

Reagents and Conditions : (i) = MeOH / KOH, - 5 - 0 C
(ii) = CH_2Cl_2 / H_2O, TBAB (20mole %)

2.2. Synthesis of NKDA - Metal Complexes

10 mmole (3.372g) of Nitroketene dithioacetal was dissolved in 20 ml of distilled water. 10 ml of aqueous solution of the metal salt M (5 mmole, where M = ($CoCl_2.6H_2O$, $NiCl_2.6H_2O$, $ZnCl_2.4H_2O$, $FeCl_3$ and $CuCl_2$) was added to the NKDA solution. The colour change and pH were recorded. The mixture was refluxed for 5 hours and left to stand overnight. The precipitates formed were filtered, washed with distilled water and methanol [8]. The precipitate formed were stored in well-labeled containers and dried over $CaCl_2$ in a dessicator.

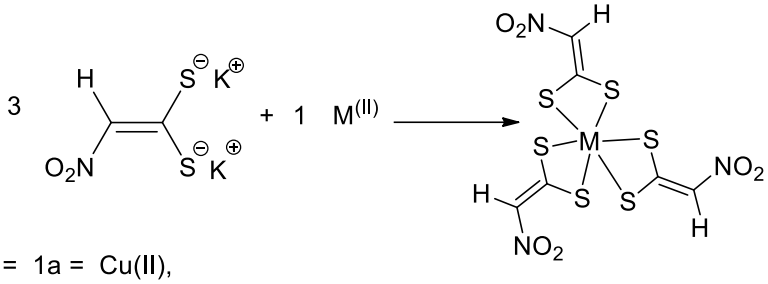

M = 1a = Cu(II),
1b = Co(II),
1c = Fe(II),
1d = Ni(II),
1e = Zn(II)

3.0. CHARACTERIZATION OF COMPLEXES

3.1. Solubility Test

The solubility of the complexes was studied in various solvents such as distilled water, ethanol, methanol, acetone, chloroform, benzene, dimethyl sulfoxide, petroleum ether.

3.2. Melting Point Test

The melting point and decomposition temperature of both the ligands and complexes were determined using the Gallenkamp apparatus at BioChemistry Department.

3.3. Thin Layer Chromatography

The thin layer chromatography of the metal salts, ligands and the complexes were carried out to determine their purity. This is based on variation in the rate of migration of the components sample. Thin layer chromatography was carried out by using a TLC plate coated with silica gel. The solution of the compounds in their respective solvents were made and spotted on the TLC plate. These were developed using a mixture of methanol and acetone (7:3) for the single NKDA complexes. After the developments, the chromatograms were dried and viewed under UV lamp at 254 nm and 336 nm respectively, in order to determine their R_f values.

3.4. Conductivity Test

The molar conductance of the complexes was determined in DMSO using HANNA instrument conductivity meter, with a cell constant of 0.83.

3.5. UV-Visible Spectroscopy

The UV-Visible spectra of the ligands and the complexes in DMSO solution were run on the Aquamate V4.60 UV/Visible spectrophotomer, at the Chemistry Department, VHNSN College, Virudhunagar.

3.6. Infrared Spectroscopy

The infrared spectra were recorded using KBr pellets with Buck Scientific M500 IR spectrophotometer at the Chemistry Department, VHNSN College, Virudhunagar.

3.7. Characterization

The crystalline structure of the NZ was characterized by powder X-ray diffraction (PXRD) by XPERT-PRO (PANalytical B.V., The Netherlands) diffractometer (Cu Kα radiation, λ=1.54 Å). The morphology of the as-synthesized NZ was studied by scanning electron microscopy (SEM) at room temperature (25 ºC) using SEM (Hitachi S-3000 H).

3.8. Fabrication of NZ/SPCE

As-synthesized NZ was firstly dispersed in water (0.05 mg mL^{-1}), and keep in ultra-sonication treatment for 60 min. On surface of SPCE, the optimized the concentration of about 8 µL of a dispersed solution was drop cast on the energetic surface of the SPCE followed by dried in an air oven at 30 °C for 1 h.

4.0. Structural characterization of products (1a – 1e)

4.1. Structural characterization of product 1a

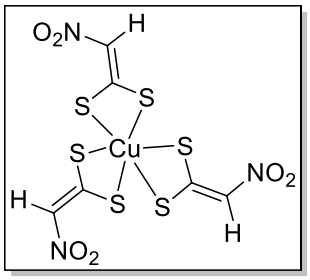

Rf = 0.62 (90:10 hexane : ethyl acetate) MP = 244-246 ˚C; Yield: 56.4% UV (methanol) λmax 580 nm; IR(nujol) ν 617 **(**C-S), 629 (C-H), 1653(C=C), 1398(C-NO_2), 3767(M-S), 1455(N-CH=C), 1121(C-N Stretch), 1115(N-O Stretching) cm^{-1}; ^1H NMR (300 MHz, CDCl3) δ 6.70 (s, 3H) ppm; ^{13}C NMR (75 MHz, CDCl3) δ113.6 (olefinic-C), 146.1(quaternary =C) ppm. MS (*m/z*): 465 (M+); Anal. Calcd for: C, 33.2; H, 6.05; N, 6.47, Cu, 9.78, O, 14.78, S, 29.6;Found: C, 33.45; H, 6.26; N, 6.53, Cu, 9.46, O,14.89, S, 28.98.

4.2. Structural characterization of product 1b

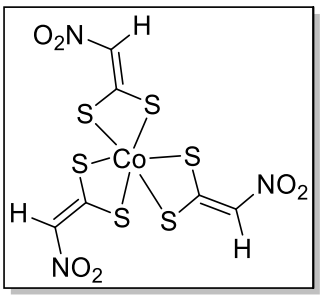

Rf = 0.60 (90:10 hexane : ethyl acetate) MP = 260-262 ˚C; Yield: 52.0% UV (methanol) λmax 580 nm; IR(nujol) ν 628 **(**C-S), 631 (C-H), 1652(C=C), 1395(C-NO_2), 3755(M-S), 1464(N-CH=C), 1139(C-N Stretch), 1149(N-O Stretching) cm^{-1}; ^1H NMR (300 MHz, CDCl3) δ 6.70 (s, 3H) ppm; ^{13}C NMR (75 MHz, CDCl3) δ113.6 (olefinic-C), 146.1(quaternary =C) ppm. MS (*m/z*): 463 (M+); Anal. Calcd for: C, 36.9; H, 6.71; N, 7.17, Co, 26.76, O, 16.38, S, 32.8;Found: C, 36.45; H, 6.26; N, 7.53, Co, 25.9, O,16.89, S, 32.98.

4.3.. Structural characterization of product 1c

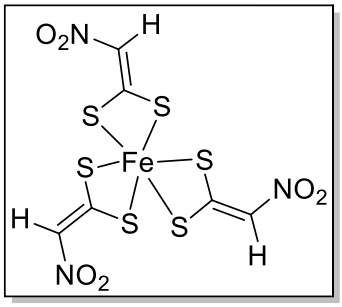

Rf = 0.60 (90:10 hexane : ethyl acetate) MP = 260-262 ˚C; Yield: 52.0% UV (methanol) λmax 580 nm; IR(nujol) ν 628 **(**C-S), 631 (C-H), 1652(C=C), 1395(C-NO_2), 3755(M-S), 1464(N-CH=C), 1139(C-N Stretch), 1149(N-O Stretching) cm^{-1}; ^1H NMR (300 MHz, CDCl3) δ 6.70 (s, 3H) ppm; ^{13}C NMR (75 MHz, CDCl3) δ113.6 (olefinic-C), 146.1(quaternary =C) ppm. MS (*m/z*): 4630(M+); Anal. Calcd for: C, 33.69; H, 6.13; N, 6.55, Fe, 8.70, O, 14.96, S, 29.9;Found: C, 33.45; H, 6.26; N, 6.53, Fe, 8.92, O,14.89, S, 29.98.

4.4. Structural characterization of product 1d

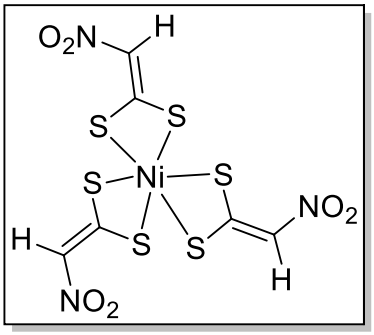

Rf = 0.70 (90:10 hexane : ethyl acetate) MP = 272-274 ˚C; Yield: 45.6% UV (methanol) λmax 560,650 nm; IR(nujol) ν 629 **(**C-S), 649 (C-H), 1657(C=C), 1395(C-NO_2), 3750(M-S), 1450(N-CH=C), 1129(C-N Stretch), 1111(N-O Stretching) cm^{-1}; ^1H NMR (300 MHz, CDCl3) δ 6.70 (s, 3H) ppm; ^{13}C NMR (75 MHz, CDCl3) δ113.6 (olefinic-C), 146.1(quaternary =C) ppm. MS (*m/z*): 463(M+); Anal. Calcd for: C, 33.5; H, 6.10; N, 6.52, Ni, 9.11, O, 14.89, S, 29.8;Found: C, 33.45; H, 6.26; N, 6.53, Ni, 9.42, O,14.78, S, 29.28.

4..5. Structural characterization of product 1e

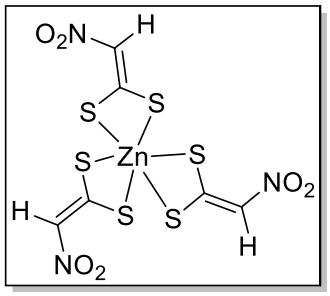

Rf = 0.64 (90:10 hexane : ethyl acetate) MP = 280-282 ˚C; Yield: 48.8% UV (methanol) λmax 570,650 nm; IR(nujol) ν 626 **(**C-S), 695 (C-H), 1639(C=C), 1318(C-NO_2), 3748(M-S), 1410(N-CH=C), 1139(C-N Stretch), 1124(N-O Stretching) cm^{-1}; ^1H NMR (300 MHz, CDCl3) δ 6.70 (s, 3H) ppm; ^{13}C NMR (75 MHz, CDCl3) δ113.6 (olefinic-C), 146.1(quaternary =C) ppm. MS (*m/z*): 468(M+); Anal. Calcd for: C, 33.1; H, 6.04; N, 6.45, Zn, 10.01, O, 14.78, S, 29.5;Found: C, 33.45; H, 6.26; N, 6.53, Zn, 9.42, O,14.18, S, 29.28.

5.0. RESULTS AND DISCUSSION:

Electronic spectra of complexes display very strong absorption band near 560-660 nm assigned to charge transfer band. This absorption band can be assigned to a charge transfer transition. It has to be mentioned that in the visible range two absorptions are observed for Co-NKDA complex at 580 and 660 nm. With no doubts, these bands are due to the d–d transitions of the planar complex. Similarly, the square planar Ni (II)-NKDA complex obtained in the aqueous solution shows two transitions at 560 and 650 nm. These d–d transitions cause that the discussed compounds are brown. Copper (II) complex shows a broad absorption band at 580 nm (21739 cm^{-1}) which can be assigned to d-d transition corresponding to 2T2g - 2Eg. As expected for a d^{10} electronic configuration, the electronic spectrum of zinc (II) complex does not show any d-d transition. The observed bands are due to the ligand and charge transfer transitions. The bands at 650 nm are assigned to n - Π* transition. The other band located at 579 nm is assigned to charge transfer transition. The yellow color of the complex may be conjured as having arisen from this absorption in the visible region. Iron(III), deduced as a high spin(d^5) complex based on its magnetic susceptibility, shows a very broad band around 655 nm which can be assigned to spin forbidden d-d transition as well as charge transfer transitions. The infrared spectra of Co (II), Ni (II), Zn (II), Fe (II) and Cu (II) complexes of Nitroketene dithioacetal are shown in Table 3. The IR spectrum of the free NKDA was compared with those of its complexes to determine the coordination sites at which the nitrokentene dithioacetal coordinated to the metal ions. The IR spectrum of NKDA showed a strong peak at 1410 cm^{-1} which were assigned to N-CH=C stretching vibrations. These peaks have been shifted in the metal complexes. The strong broad band at 650 cm^{-1} due to C-H (sp^2 CH bend), observed in the free NKDA is also present in all the complexes. This band remains unchanged upon complexation although slightly shifted in most of the complexes. The weak absorption band at 1100 cm^{-1} due to C-N stretching of NKDA has been shifted in the metal complexes. The weak absorption band at 700 cm^{-1} due to C-S stretching of NKDA has been shifted in the metal complexes showing that the metal ion is likely to coordinate to the ligand through this point. Some new medium bands around 3746 cm^{-1} and 3767 cm^{-1} in most of the complexes, were tentatively assigned to (M-S) vibrations. Infrared spectral bands of ligand (NKDA) observed at 1170 cm^{-1} (ν N-O) and at 1410 cm^{-1} (ν N-CH=C) remained almost unchanged in position on complexation indicating absence of bonding through nitrogen. However,(ν C-S) of the ligand undergoes red shift of 70- 80 cm^{-1} on complexation indicating bonding through sulphur in all complexes.The systematic shift in C-S bonds of ligands clearly indicate formation of metal sulphur bond. The olefinic protons in ^{1}HNMR were appeared in the range of ~6.70 ppm for the products **1a – 1e**. Similarly in ^{13}CNMR the olefinic carbon atoms were appeared in the range of ~146.1ppm for the products 1**a – 1e**. The olefinic quaternary carbons were appeared in the range between ~113ppm for the products **1a – 1e**. C, H, N elemental analysis data for the products **1a – 1e** showed good agreement with the calculated values for the confirmation of molecular weight of the products.

Table1: Solubility Data of NKDA and its complexes

Ligand/ Complex	Distilled water		Ethanol		Methanol		Acetone		Chloroform		Benzene	
	C	H	C	H	C	H	C	H	C	H	C	H
NKDA	S	S	S	S	SS	SS	S	S	SS	SS	NS	NS
Cu(NKDA)3	NS	NS	SS	SS	SS	SS	SS	SS	NS	NS	NS NS	
Co(NKDA)3	NS	NS	SS	SS	SS	SS	SS	SS	NS	NS	NS NS	
Ni(NKDA)3	NS	NS	SS	SS	SS	SS	SS	SS	NS	NS	NS NS	
Zn(NKDA)3	NS	NS	SS	SS	SS	SS	SS	SS	NS	NS	NS NS	
Fe(NKDA)3	NS	NS	SS	SS	SS	SS	SS	SS	NS	NS	NS NS	

NB: S = Soluble, SS = Slightly soluble, NS = Not soluble, C = cold, H = hot

Table2: Some physical properties of NKDA and its complexes

Ligand/ Complex	Colour	M.pt (oC)	Rf	% yield	Conductivity Scm2mol-1	Molecular weight	Exact mass	Elemental Analysis					
								C	H	M	N	O	S
NKDA	Reddish	212	0.56	87.3	$1.20x10^{-6}$	216	215.78	31.3	7.23	----	4.57	10.44	20.9
Cu(NKDA)3	Blue	244-246	0.62	56.4	$2.50x10^{-3}$	469.04	467.76	33.2	6.05	9.78	6.47	14.78	29.6
Co(NKDA)3	Light pink	260-262	0.60	52.0	$6.15x10^{-3}$	464.43	463.77	36.9	6.71	26.76	7.17	16.38	32.8
Ni(NKDA)3	Brown	272-274	0.70	45.6	$4.22x10^{-3}$	462.77	464.19	33.5	6.10	9.11	6.52	14.89	29.8
Zn(NKDA)3	Purple	280-282	0.64	48.8	$5.10x10^{-3}$	470.87	468.76	33.1	6.04	10.01	6.45	14.78	29.5
Fe(NKDA)3	Green	268-270	0.68	53.8	$5.43x10^{-3}$	461.64	460.77	33.69	6.13	8.70	6.55	14.96	29.9

All the complexes of NKDA have higher melting points compared with the free NKDA. All the complexes are slightly soluble in acetone, DMSO, benzene and petroleum ether and insoluble in chloroform. All the complexes were obtained as powder. The complexes are of various colours. The results of the conductivity measurement indicate that all the complexes are non-electrolytes.

Table 3: Selected IR data (cm^{-1}) for NKDA and its complexes

Ligand/ Complex	υ C-S	υ C-H	υ C=C	υ C-NO2	υ M-S	υ N-CH=C	υ C-N (Stretch	υ N-O Stretching
NKDA	700(C-S stretch)	650 (sp2 CH bend)	1650	1390 symmetric (medium)	-----	1410	(1190–1130)1100	1170
$Cu(NKDA)_3$	617	629	1653	1398	3767	1455	1121	1115
$Co(NKDA)_3$	628	631	1652	1395	3755	1464	1139	1149
$Ni(NKDA)_3$	629	649	1657	1395	3750	1450	1129	1111
$Zn(NKDA)_3$	626	695	1639	1318	3748	1410	1139	1124
$Fe(NKDA)_3$	--	688	1644	1404	3746	1460	1137	1128

The infrared spectra of Co(II), Ni(II), Zn(II) , Fe(II) and Cu(II) complexes of Nitroketene dithioacetal are shown in Table 3 and Appendix I. The IR spectrum of the free NKDA was compared with those of its complexes to determine the coordination sites at which the nitrokentene dithioacetal coordinated to the metal ions. The IR spectrum of NKDA showed a strong peak at 1410 cm^{-1} which were assigned to N-CH=C stretching vibrations. These peaks have been shifted in the metal complexes. The strong broad band at 650 cm-1 due to C-H (sp2 CH bend), observed in the free NKDA is also present in all the complexes. This band remain unchanged upon complexation. Although slightly shifted in most of the complexes. The weak absorption band at 1100 cm-1 due to C-N stretching of NKDA has been shifted in the metal complexes. The weak absorption band at 700 cm-1 due to C-S stretching of NKDA has been shifted in the metal complexes showing that the metal ion is likely to coordinate to the ligand through this point. Some new medium bands around 3746 cm-1 and 3767 cm-1 in most of the complexes, were tentatively assigned to (M-S) vibrations. Infrared spectral bands of ligand (NKDA) observed at 1170 cm-1 (ν N-O) and at 1410 cm-1 (ν N-CH=C) remained almost unchanged in position on complexation indicating absence of bonding through nitrogen. However,(ν C-S) of the ligand undergoes red shift.of 70- 80 cm^{-1} on complexation indicating bonding through sulphur in all complexes.The systematic shift in C-S bonds of ligands clearly indicate formation of metal sulphur bond.

Table 4: UV/Vis Spectra of NKDA and its Complexes

Ligand/ Complex	Wavelength (nm)	Assignment
NKDA	324, 410	Π→Π*
Cu(NKDA)3	580	n→Π*
Co(NKDA)3	580,660	n→Π*
Ni(NKDA)3	560,650	n→Π*
Zn(NKDA)3	570,650	n→Π*
Fe(NKDA)3	655	

H^1 NMR Spectra of NKDA-Metal Complexes 1a-1e

^{1}H–NMR spectrum of the complexes were recorded in **DMSO** and compared with the ligand to confirm the binding of active sites towards the metal ion. A singlet peak in the region δ = 6.70 ppm for the CH proton.

C^{13} NMR Spectra of NKDA-Metal Complexes 1a-1e

Similarly in ^{13}CNMR the olefinic carbon atoms were appeared in the range of ~113.6ppm for the products 1a -1e. The –CH carbon peaks appeared at 146.1 ppm. The MS M+ ion peaks and C, H, N elemental

analysis data for the product 1a to 1e showed good agreement with the calculated values for the confirmation of molecular weight of the products. EDX analysis data confirmed the presence of elements and the corresponding metals in the complexes 1a-1e. The Fab-MS M+ ion peaks and C, H, N elemental analysis data for the product 1a to 1e showed good agreement with the calculated values for the confirmation of molecular weight of the products. EDX analysis data confirmed the presence of elements and the corresponding metals in the complexes 1a-1e.

PXRD measurements were carried out to examine the phase and structure of the as-synthesized sample. As shown in Figure. 1A, the PXRD pattern of the as-synthesized NZ shows a broad line parallel to the amorphous nature appears at a 2θ range between 15-30°. The surface morphology of the NZ was observed by scanning electron microscopy. Figure 1 (B, and C) shows the different magnification of SEM images of a NZ is provided. From these images we confirmed that the as-synthesized NZ is in nanoparticle size.

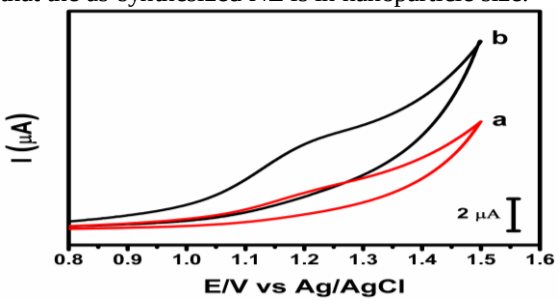

Fig. 1: (A) PXRD, (B, and C) SEM image of (Zn(NKDA)$_3$)

6.0. Electro-oxidation of L-Met at NZ/SPCE

The electro-oxidation activity of the bare SPCE, and modified SPCE was observed by Cyclic Voltammetry (CVs). Figure. 2A shows the CV curves of different electrodes such as (a) bare SPCE presence of 200 µM L-Met, and (b) NZ/SPCE with 200 µM of L-Met in PBS (pH 7) at the scanning rate of 50 mV s^{-1}. There is no peak appeared when introduced SPCE into the electrochemical setup. In the addition of L-Met in bare SPCE a shows small difference in the CV curve with a small peak potential (1.228 V) at E_{pa} (anodic peak potential) with a small current. The well-marked anodic peak potential (E_{pa}) were detected at 1.196 V for the NZ/SPCE as shown in Figure. 2A. The results show that the electrochemical behavior of L-Met has an irreversible and oxidation-oxidation process. However relatively, NZ/SPCE is showed maximum electro-oxidation performance compared to bare SPCE in terms of high peak currents, and less over potential. Thus, NZ/SPCE has a greater electro-oxidation ability to the oxidation of L-Met[32,33,34] due to the perfect synergy between big surface area, and high conductivity of the excellent electro-oxidation capability of NZ. The huge anodic peaks happen at peak potentials of 1.196 V due to $2e^-$ oxidation of the L-Met. The L-Met molecules were absorbed by the modified electrode and are oxidized at 1.196 V. The CV curves definitely authorizes that the NZ/SPCE is a good electrochemical detection of L-Met.[35-42]

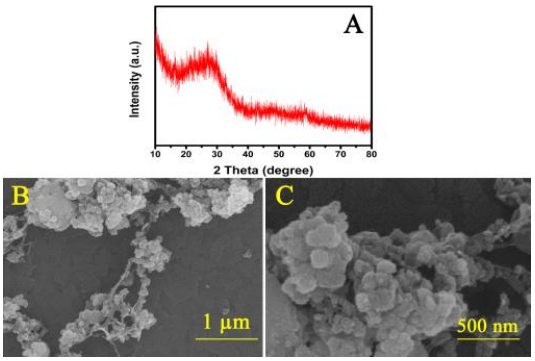

Fig. 2: (A)CVs response of (a) bare GCE with 200 µM L-Met
(b) NZ/SPCE with 200 µM L-Met in 0.05 M PBS(pH 7)

6.1. Effect of concentrations and scan rates

Figure. 3A shows CV responses of NZ/SPCE in PBS containing different concentrations of L-Met at a scanning rate of 50 mVs^{-1}. When the absence of L-Met (a), the NZ/SPCE does not show any discernible peaks; whereas a well-defined oxidation peak was observed in the presence of 100µM of L-Met. Additionally, the oxidation peaks current of the L-Met increases with increasing the L-Met concentrations from 100 to 1000 µM of L-Met (a-j). The results reveals that the excellent electro-oxidation behavior of L-Met at NZ/SPCE and can be used for sensitive determination of L-Met.[43-46] Figure. 3B demonstrates the plot between oxidation peak current and the concentration of L-Met, which may be communicated by a linear regression equation as E_{pa} (V) = 16.009x – 1.3572 0.996, R^2 = 0.996.

Figure. 3C shows that the effect of scanning rate of electro-oxidation responses of NZ/SPCE in PBS (pH 7) for the determination of L-Met. The CV curves observed the oxidation peaks currents are gradually increased when increasing the anodic peaks from 20 to 200 mVs^{-1}. When the oxidation peaks current (I_{pa}) increases the scan rate also increases linearly. Additionally, the inset linear plot among oxidation peak current versus the square root of the scan rates has displayed a relationship which suggesting that the oxidation process of L-Met appeared at the NZ/SPCE is a diffusion controlled electron transfer process (Figure. 3D). From the results, we approve that the observed CV reports are due to the determination of

L-Met diffused on the surface of the NZ/SPCE. Figure. 3D demonstrates the plot between oxidation peak current and the square root of scan rate, which may be communicated by a linear regression equation as E_{pa} (V) = 0.7243x – 3.4794, R^2 = 0.9906. The above results are clearly confirming that the process is a diffusion controlled irreversible process.

LOD=3S_b/b ------- 1

The LOD is calculated by using the above formula, slope of the straight line of the electrochemical analytical curve and SD of the mean value for seven voltammograms of the blank (S_b).

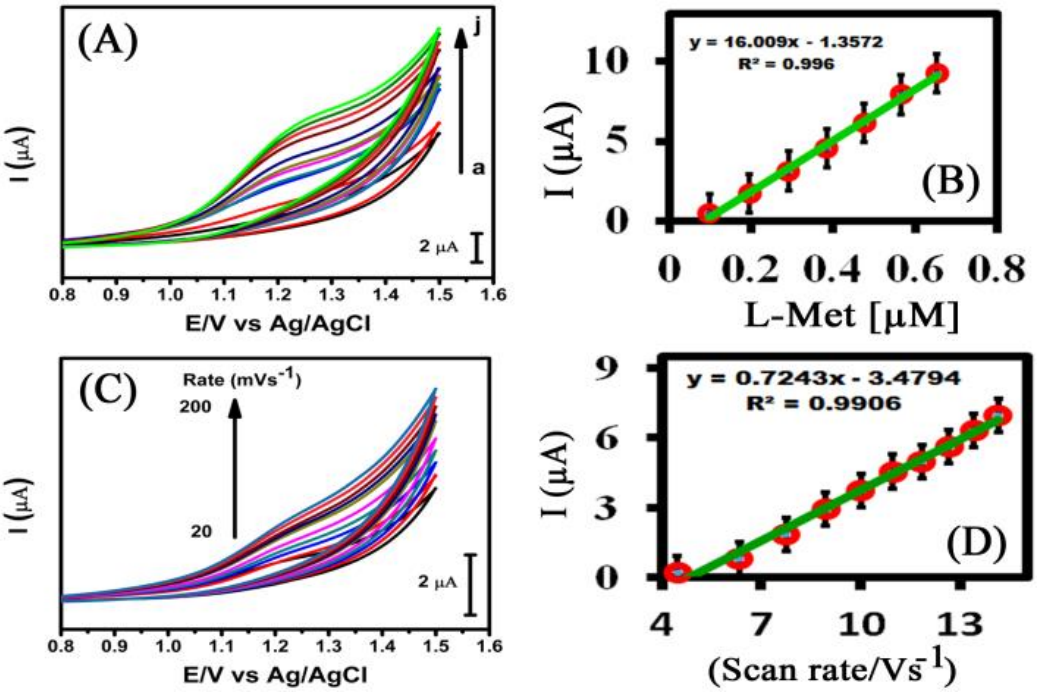

Fig. 3: (A) CVs of NZ/SPCE in PBS (pH 7) in the presence of L-Met with different concentrations (a-j = 100-1000 µM L-Met) at a scan rate of 50 mV s^{-1}, (B) The plot between oxidation peak current and the concentration of L-Met, (C) CVs obtained at NZ/SPCE in PBS (pH 7) containing 200 µM L-Met at different scan rates (20 to 200 mV s^{-1}), and (D) The plot between oxidation peak current, and the square root of scan rate.

6.2. Electrochemical oxidation of L-Met

The electrochemical oxidation of L-Met was done at NZ/SPCE by DPV[20,21]. The DPV technique is a more sensitive method for the detection of L-Met than CV. The DPV responses of the NZ/SPCE with the additions of various concentration of L-Met (6-8347 µM) into the PBS (pH 7). The sensitivity was calculated by using the slope of the calibration plot as shown in the Figure. 4. The calculated sensitivity was about 2.8002 (±0.002) µA μM^{-1} cm^{-2} and limit of detection (LOD) is 50.1 µM. A linear relationship between L-Met concentration vs peak current (I_{pa}) was obtained using 6-8347 µM of L-Met, and a linear regression values and correlation coefficient as *I*pa (V) = 0.1562x – 0.1016 and R^2 = 0.993 respectively. The detection limit was 50.1 µM observed from the slope of the calibration plot, as shown in the Figure. 4.

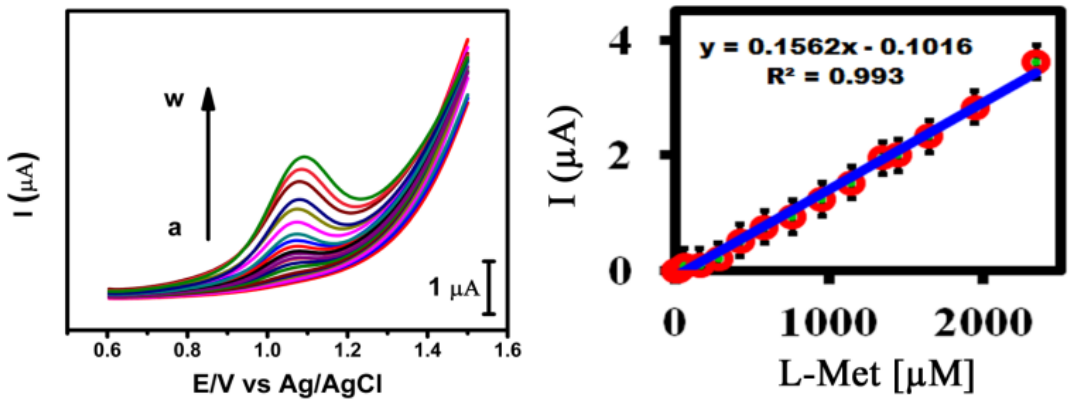

Fig. 4: DPVs of NZ/SPCE towards increasing concentration of L-Met in PBS (pH 7) (a to w = 6-8347 µM), and calibration plot.

6.3. Stability, reproducibility and repeatability

In order to examine storage stability of the NZ/SPCE, its electro-catalytic answer towards L-Met (100 µM) is checked up to one week of the storage period, the catalytic current slightly decreased, while 94.62% of the initial response current was engaged which exposes good storage stability of the film. Additionally, the electrode displays considerable repeatability with RSD of 3.51% for five repetitive measurements carried out using single electrode and it exhibits considerable reproducibility with RSD of 3.21% for five independent measurements carried out in five different electrodes.

7.0. Antibacterial activity studies of NKDA-Metal complexes 1a-1e

The anti bacterial activity screening for NKDA – Metal complexes were determined by invitro Disc-Diffusion method. The antibacterial activity studies in nutrient agar medium for the following gram+ve and gram-ve organisms *Escherichia coli, Proteus sp, Serratiamarcescens, Pseudomonas aureginosa, Citrobactorsp, Klebsiella pneumonia, Bacillus subtills, Micrococcus, Staphylococcusaureus* and *Streptococcus viridians* were carried out. The results were tabulated and compared with the standard drug sulfadiazine.

7.1.Materials and Methods:

Analar grade chemicals, sterile empty disc and 300µg standard sulfadiazine disc used for the study were purchased from HIMEDIA chemicals. SIGMA micropipette was used to load 300 µg of NKDA. The culture preparation was carried out in bio safety Bio Technics laminar air flow chamber.

7.2. Preparation of nutrient agar medium

Exactly 1g of peptone 0.5g of Beef extract and 0.5 g of sodium chloride were weighed and transferred into conical flask and dissolved in 100ml of distilled water after the pH range was checked for 7.0 – 7.2 , finally added 1.5 g of agar into the conical flask. It was closely packed with cotton plug and placed in an autoclave for 15 minutes for sterilization. 100mL of nutrient agar medium was poured into the petri plates and allowed for solidification without any disturbance. The test organism was lawned on the surface of the agar medium using a cotton swap. The concentration of 300µg of NKDA – Metal complexes was loaded on the empty disc using micropipette. The loaded sterile disc was placed on the culture lawned nutrient agar medium in the petri plate and incubated in the inverted position for 16-18 hours at 35°C. 300µg of sulfadiazine disc was used as standard drug.

7.3. Results and Discussion:

The antibacterial activity studies in nutrient agar medium for the following gram+ve and gram-ve organisms *Escherichia coli, Proteus sp, Serratiamarcescens, Pseudomonas aureginosa, Citrobactorsp, Klebsiella pneumonia, Bacillus subtills, Micrococcus, Staphylococcusaureus and Streptococcus viridians* were carried out and the results were tabulated in Table – 5. From the results it is found and reported that NKDA – Metal complexes was exhibiting anti bacterial activity in the form of zone of inhibition.

Table 5: Antibacterial activity of NKDA – Metal complexes 1a-1e

Name of the Culture	Zone of Inhibition in mm for Products (1a-1e)					Standard
	1a	1b	1c	1d	1e	Sulfadiazine
Escherichia coli	**18**	16	**17**	**19**	9	24
Proteus sp.	**16**	9	**13**	**15**	11	19
Serratiamarcescens	**14**	15	**14**	**14**	7	20
Pseudomonas aeruginosa	**17**	14	**17**	**14**	14	22
Citrobactor sp.	**14**	10	**16**	**14**	12	21
Klebsiella pneumonia	**15**	12	**17**	**14**	12	18
Bacillus subtilis	19	**21**	12	17	**21**	27
Micrococcus	17	**20**	14	19	**19**	26
Staphylococcus aureus	21	**19**	19	23	**21**	31
Streptococcus viridans	20	**24**	15	21	**18**	29

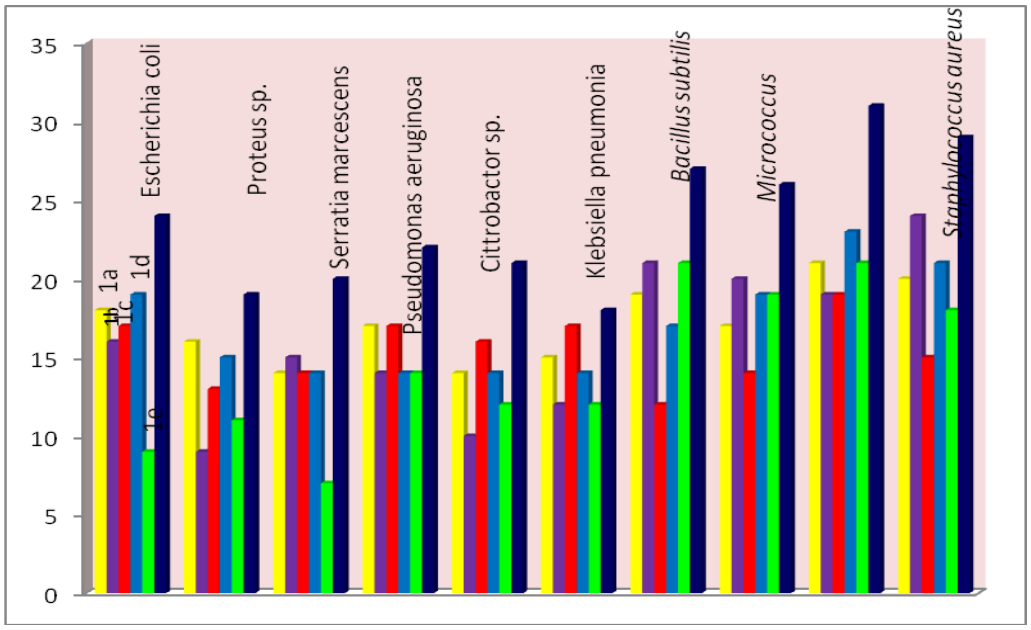

From the measured results in the form of zone of inhibition in mm, it is found and reported that the complexes 1a, 1d, showed potent antibacterial activity against gram-ve *Escherichia coli* bacterial strains compare to the standard drug sulphadiazine. The complexes 1a, 1c, 1d, showed potent antibacterial activity against gram+ve *Staphylococcus aureus* bacterial strains compare to the standard drug sulfadiazine. The complexes 1c showed moderate antibacterial activity against gram+ve bacterial strains compare to the standard drug sulfadiazine.

8.0. Central nervous system depressant activity studies of NKDA-Metal complexes 1a-1e

Based on the fundamental report, we have planned to extend the CNS depressant activity study for NKDA – Metal complexes using Albino mice animal screening protocols in Actophotometer. The central nervous system depressant activity in Albino mice animal screening experiment was done by following the pharmacological protocol as reported by Kulkarni.et.al. The CNS activity can be experimentally measured by using Actophotometer equipment which operates with the help of photo electric cells which are connected in circuit with a counter. When a beam of light falling on the photo cell is cut off by the animal due to the animals change in locomotor activity a count is recorded in Actophotometer.

8.1. Materials and methods

Analar grade of carboxymethyl cellulose powder was used in all the study. Locomotor activity of Albino mice was determined using digital Actophotometer, Besto make, Haryana. All animal experiments were carried out by following the guidelines of CPCSEA. The animal ethical committee approved to conduct the animal experiments (IAEC/ CPCSEA/1086/07 dated 27-10-2007).

Table – 6.0. –Cumulative locomotor activity results of NKDA -Metal complexes				
Product number	Dose	Locomotor activity score for 10 minutes		% of CNS depressant activity
		Before treatment	After treatment	
Control	2mg cmc / 5mL H_2O	188.833±39.06[a]	165.666±39.24[a]	12.166±1.04[d]
Chlorpromazine	3mg	124.666±69.39[a]	84.833±23.51[b]	31.523±2.59[i,j]
NKDA	10mg	206.333±65.22[a]	168.00±39.75[c]	19.484±2.69[f]
1a	10mg	197.16±47.39[a]	79.83±23.62[b]	59.67±1.70[h,i]
1b	10mg	214.00±68.47[a]	90.83±31.18[b]	57.78±1.91[g,h]
1c	10mg	246±58.23[a]	64.66±11.62[b]	73.65±22.59[i,j]
1d	10mg	210.67±59.83[a]	85.17±26.27[b]	59.68±1.70[h,i]
1e	10mg	205.50±50.57[a]	140.83±38.98[c]	31.85±2.53[e]

Actophotometer

Requirement:

Animal = Albino Mice[35-50g]
Equipment = Actophotometer[BESTO]

The CNS activity can be easily measured by using Actophotometer equipment which operates with the help of photo electric cells which are connected in circuit with a counter.When a beam of light falling on the photo cell is cut of by the animal,a count is recorded an Acto photometer could have either circular or square arena in which the animal moves .

8.2. Animals used

Albino mice of both sexes of weight ranges between 25g and 45g were used for CNS depressant activity study. The animals were kept in torsion polypropylene cages in a room maintained under controlled atmospheric conditions. The animals were fed with standard diet and kept in dark/light cycle 12hrs/12hrs and drinking water ad libitum.

8.3. Preparation of dose and Route of Administration

The dose concentration of 10mg of NKDA – Metal complex, 5mL of distilled water and 2 mg of carboxymethyl cellulose (CMC) powder was weighed and taken in a morter and pestle. The mixture was triturated well to convert the solution as a gel. From this bulk gel, doses for individual animal was taken based upon the animal body weight and fed to the animal orally using an oral canal.

8.4. Results and Discussion:

The animals were divided into 7 groups. Six animals were taken in each group (n= 6). Each albino mice was weighed in a physical balance and marked individually. Initially all the animals were placed in the Digital actophotometer activity cage (Size of 36 x 37cm) for 10 minutes to determine the basal locomotor activity score. Animals of Group–1 are served as control and treated with 2mg of carboxy methyl cellulose in 5mL of distilled water. Animals of Group-2 were orally treated with the standard drug Chlorpromazine 3mg/kg, (i.p.) using a oral canal. Animals in between Group-3 and Group-7 were orally treated with NKDA-Metal complexes based on the animal body weight in the form of well triturated gel prepared using 5mL of distilled water, 10mg of NKDA – Metal complex and 2mg of carboxy methyl cellulose. All the animals were left freely in the animal cage for 30 minutes for the absorption of drugs. The locomotor activity score for all the

animals were again determined for all the 5 Group animals after the drug absorption. The percentage of CNS depressant activity was calculated using the formula

$$\% \text{ of CNS depressant activity} = \frac{A - B}{A}$$

A = locomotor activity score before drug treatment

B = locomotor activity score after drug treatment

The Mean change in locomotor activity score recorded for each group of animals were calculated The percentage of CNS depressant activity of NKDA – Metal complexes was compared with standard drug chlorpromazine and the results were statistically analyzed using Statistical Package for the Social Sciences (SPSS 12.0). The data were analysed with ANOVA and Duncan's multiple range test (DMRT). The data are expressed as mean±SD, for 6 animals in each group. From the results it is found and reported that NKDA was exhibiting CNS depressant activity.

8.0. CONCLUSION:

In this paper we have reported the synthesis of NKDA – Metal complexes. The structure of NKDA – Metal complexes was characterized using UV, IR, ^{1}HNMR, ^{13}CNMR, C,H,N elemental analysis, EDX analysis and Fab mass spectral evidences. In this paper we have reported the results of antibacterial study of NKDA – Metal complexes. From the measured results in the form of zone of inhibition in mm, it is found and reported that NKDA – Metal complexes showed potent antibacterial activity against gram-ve bacterial strains compare to the standard drug sulphadiazine. NKDA – Metal complexes showed antibacterial activity against both gram–ve and gram+ve bacterial strains compare to the standard drug sulfadiazine. In future this class of products with nitroketenedithioacetal motif may be used as good therapeutic drugs against bacterial borne diseases in mankind. In this paper we have reported the central nervous system depressant activity study of NKDA – Metal complexes using Albino mice animal screening experiment and the results were analysed with ANOVA and Duncan's multiple range test (DMRT) using SPSS.12 version. The data are expressed as mean±SD, for 6 animals in each group. The results were compared with the standard drug chlorpromazine. Among them, NKDA – Metal complexes showed significant CNS depressant activity compare to the standard drug chlorpromazine. In this paper NKDA – Zinc complex was prepared and characterized by X-ray diffraction (XRD), scanning electron microscopy (SEM) which showed that the agglomeration in structure. The as-synthesized NZ has high dispersible property in water. The modified SPCE of NZ have electro-catalytic activity towards the detection of L-Met. The electrochemical behavior of the NZ/SPCE were examined using cyclic voltammetry, and differential pulse voltammetry (DPV). From the electrochemical study, the limit of detection, sensitivity, and linear range are 50.1 µM, 2.8002 (±0.002) µA μM^{-1} cm^{-2}, and 6-8347 µM. The assembled sensor exhibits a tremendous electro-catalytic performance with a low limit of detection and good sensitivity property.

ACKNOWLEDGEMENT:

The author sincerely thanks to Tamilnadu State Council for Science and Technology – Students Project Scheme 2017-2018 for providing fund for carryin out this project successfully. The authors sincerely thanks to the management of V.V. Vanniaperumal College for Women, Virudhunagar for providing necessary facilities and constant encouragement.

REFERENCES:

1. Jain, K.K. Applications of nanobiotechnology in clinical diagnostics. *Clin. Chem*. **2007;***53:*2002–2009.

2.Jain, K.K. Nanomedicine: Application of nanobiotechnology in medical practice. *Med. Princ.Pract.* **2008;** *17:* 89–101.

3. Zhao, W.; Karp, J.M.; Ferrari, M.; Serda, R. Bioengineering nanotechnology: Towards the clinic.*Nanotechnology* **2011;** *22:* doi:10.1088/0957-4484/22/49/490201.

4. Conde, J; Rosa, J.; Lima, J.C.; Baptista, P.V. Nanophotonics for Molecular Diagnostics and Therapy Applications. *Int. J. Photoenergy*. **2011;** *2012*, 619530, doi:10.1155/2012/619530.

5. Baptista, P.V.; Doria, G.; Quaresma, P.; Cavadas, M.; Neves, C.S.; Gomes, I.; Eaton, P.

6. Synthesis, characterization and antibacterial activity of alkyl, benzyl and chloro substituted benzyl derivatives of nitroketene dithioacetals L. Sakthikumar, J. Kavitha and R. Mahalakshmi, Der Pharma Chemica, 2014, 6(2):294-298

7. Electro-oxidation and Determination of Sulfur-containing Amino Acid on Screen-printed Carbon Electrode Modified with NZ Kavitha J, Mahalakshmi R. Der Pharma Chemica, 2017, 9(12):70-75.

8. Synthesis,spectral and biological studies of mixed ligand transition metal complexes of nitroketene dithioacetal with ephedrine, J. Kavitha, L. Sakthikumar, R. Mahalakshmy. Indo American Journal of Pharmaceutical Sciences, IAJPS 2018; 05 (01): 645-658 , ISSN 2349-7750

9. Azzazy, H.M.; Mansour, M.M. *In vitro* diagnostic prospects of nanoparticles. *Clin. Chim. Acta* 2009; *40:*, 1-8.
10. Baptista, P.V.; Doria, G.; Quaresma, P.; Cavadas, M.; Neves, C.S.; Gomes, I.; Eaton, P.
11. Larguinho, M.; Baptista, P.V. Gold and silver nanoparticles for clinical diagnostics—From genomics to proteomics. *J. Proteomics* 2011, in press. *Sensors* 2012, *12* 1676.
12. Conde, J.; Doria, G.; Baptista, P. Noble metal nanoparticles applications in cancer. *J. Drug. Deliv.***2012;** *2012*, doi:10.1155/2012/751075.
13. Eggins, B. R. (1996). Biosensors: an introduction, Wiley.
14. Dzyadevych, S. V.; Arkhypova, V. N.; Soldatkin, A. P.; El'skaya, A. V.; Martelet, C. & Jaffrezic-Renault, N. (2008). Amperometric enzyme biosensors: Past, present and future. *Irbm* 29, 171-180.
15. R. Prabhakar, Bandaru, Electrical properties and applications of carbon nanotube structures, J. Nanosci. Nanotechnol. 2007;7: 1239-1267.
16. V. Q. Nguyen, D. Schaming, P. Martin, J. C. Lacroix, Highly resolved nanostructured PEDOT on large areas by nanosphere lithography and electrodeposition, ACS Appl. Mater. Interfaces.2015; 7: 21673−21681.
17. M. Raissan, A. Bahrani, X. Xu, W. Ahmada, X. Ren, J. Su, Z. Cheng, Y. Gao, Highly efficient dye-sensitized solar cell with GNS/MWCNT/PANI as a counter electrode, Mater Res Bull. 2014;59: 272-277.
18. H. Sun, M. Ahmad, J. Zhu, Morphology-controlled synthesis of Co_3O_4 porous nanostructures for the application as lithium-ion battery, Electrochim. Acta. 2013; 89:199-205.
19. M. Ahamad, S. Yingying, A. Nisar, H. Sun, W. Shen, M. Wei, J. Zhu, Synthesis of hierarchical flower-like ZnO nanostructures and their functionalization by Au nanoparticles for improved photocatalytic and high performance Li-ion battery anodes, J. Mater. Chem.2011; 21: 7723-7729.
20. U. Diebold, Structure and properties of TiO_2 surfaces: a brief review, Appl. Phys. A: Mater. Sci. Process. 2003;76: 681-687.
21. H. J. Zeiger, T. A. Kaplan, P. Raccah, Semiconductor-metal transition in Ti_2O_3, Phys. Rev. Lett. 1971;26: 1328-1331.
22. Z. Weng, H. Guo, X. Liu, S. Wu, K. Yeung, P. K. Chu, Nanostructured TiO_2 for energy conversion and storage, RSC Adv.2013; 3:24758-24775.
23. H. Cheng, J. Ma, Z. Zhao, L. Qi, Hydrothermal preparation of uniform nanosize rutile and anatase particles, Chem. Mater.1995; 7: 663-671.